Concept for controlled transverse emittance transfer within a linac ion beam

L. Groening

GSI Helmholtzzentrum für Schwerionenforschung GmbH, Planckstrasse 1, D-64291 Darmstadt, Germany

(Received 31 January 2011; published 29 June 2011)

For injection of beams into circular machines with different horizontal and vertical emittance acceptance, the injection efficiency can be increased if these beams are flat, i.e., if they feature unequal transverse emittances. Generation of flat electron beams is well known and has been demonstrated already in beam experiments. It was proposed also for ion beams that were generated in an electron-cyclotron-resonance (ECR) source. We introduce an extension of the method to beams that underwent charge state stripping without requiring their generation inside an ECR source. Results from multiparticle simulations are presented to demonstrate the validity of the method.

DOI: 10.1103/PhysRevSTAB.14.064201 PACS numbers: 41.75.Ak, 41.85.Ct, 41.85.Ja

I. INTRODUCTION

Beams provided by linacs generally have equal or quite similar horizontal and vertical emittances (ϵ_x and ϵ_y). If beams from linacs are to be injected into a subsequent circular machine, the injection process might impose different acceptance limits ($A_x < A_y$) on the two transverse emittances. One common injection scheme is the multiturn injection using a time dependent orbit bump in one plane for beam stacking in this plane. As a consequence, the injected beam emittance in this plane, the horizontal for instance, must be significantly lower with respect to the other one. To meet the acceptance criteria in both planes, linac designers and operators try to keep both transverse emittances below the more stringent acceptance limit:

$$\epsilon_x \cdot \epsilon_y = \epsilon_x^2 < A_x^2. \tag{1}$$

The requirement to the product of the emittances is relaxed if the linac beam will feature different transverse emittances as well, i.e., emittances being adopted to the acceptances of the machine into which injection has to be performed:

$$A_x^2 < \epsilon_x \cdot \epsilon_y < A_x \cdot A_y. \tag{2}$$

To this end, a single pass beam line is needed that provides transformation of a round uncorrelated beam ($\epsilon_x = \epsilon_y$) to a flat beam ($\epsilon_x < \epsilon_y$). Although for electrons round to flat transfer was proposed [1] and has been demonstrated experimentally [2], to our knowledge it has not been proposed for initially uncorrelated round ion beams. Such an ion beam line must be different from an emittance swapping beam line that exchanges the two different transverse emittances by using three skew quadrupoles, for instance [3,4].

II. REQUIRED MATHEMATICAL TOOLS

A round to flat transformation implies beam line elements that cause coupling of the horizontal and vertical plane. It needs a four-dimensional description. This section introduces the quantities referred to in the paper. The next section deals with a conceptual layout of a round to flat transformation for ions extracted from an electron-cyclotron-resonance (ECR) source. Finally, a concept is presented that provides round to flat transformation for any uncorrelated ion beam being charge state stripped during transportation. GSI aims at experimental verification of the concepts. Multiparticle simulations were done for sections planned to be integrated into the existing universal linear accelerator (UNILAC) at GSI. Any round to flat operation should only use beam line elements being linear in the four-dimensional transverse phase space. In that case the transportation M of single particle coordinates from a position 1 to a position 2 is

$$\begin{bmatrix} x \\ x' \\ y \\ y' \end{bmatrix}_2 = \begin{bmatrix} m_{11} & m_{12} & m_{13} & m_{14} \\ m_{21} & m_{22} & m_{23} & m_{24} \\ m_{31} & m_{32} & m_{33} & m_{34} \\ m_{41} & m_{42} & m_{43} & m_{44} \end{bmatrix} \begin{bmatrix} x \\ x' \\ y \\ y' \end{bmatrix}_1. \tag{4}$$

As coordinates we use (x, y) to indicate transverse displacements and (x', y') to indicate their derivatives with respect to (wrt) the position s along the design orbit. In the following sections we refer to beam dynamics simulation results from a code that also uses these coordinates. Additionally, the experimental proof of principles will be based on measurements of these coordinates. For these reasons, we do not use the conjugate coordinates that additionally include the contribution of the magnetic vector field $\vec{A}$ in the momenta.

The linear transport preserves the four-dimensional rms emittance defined through the beam's second moment matrix,

$$C = \begin{bmatrix} \langle xx \rangle & \langle xx' \rangle & \langle xy \rangle & \langle xy' \rangle \\ \langle x'x \rangle & \langle x'x' \rangle & \langle x'y \rangle & \langle x'y' \rangle \\ \langle yx \rangle & \langle yx' \rangle & \langle yy \rangle & \langle yy' \rangle \\ \langle y'x \rangle & \langle y'x' \rangle & \langle y'y \rangle & \langle y'y' \rangle \end{bmatrix}, \tag{5}$$

and

$$\epsilon_{4d}^2 = \det C. \tag{6}$$

Second moments of the beam are transported using the matrix equation

$$C_2 = MC_1M^T. \tag{7}$$

Coupling between the horizontal and the vertical plane results in

$$\epsilon_x \cdot \epsilon_y \geq \epsilon_{4d} \tag{8}$$

with equality just for zero interplane coupling moments. Here ϵ_x and ϵ_y are the rms emittances defined through the beam moments in their sub-phase spaces in an analogue way to Eq. (6). Assuming an initial round beam without any interplane correlations, the transformation into a flat beam cannot be accomplished by applying symplectic transformations only [5]. Symplectic transformations M preserve ϵ_{4d}, meet the condition

$$M^T J M = J \tag{9}$$

with

$$J := \begin{bmatrix} 0 & 1 & 0 & 0 \\ -1 & 0 & 0 & 0 \\ 0 & 0 & 0 & 1 \\ 0 & 0 & -1 & 0 \end{bmatrix}, \tag{10}$$

and may just increase both transverse emittances (ϵ_x, ϵ_y) while keeping them equal to each other.

Rigorous analysis of coupled four-dimensional transverse beam dynamics can be found in [6–9]. This section is concluded in providing eidetic justification for the beam line elements, which a round to flat transformation should include. In order to achieve emittance reduction in one plane, the horizontal for instance, a nonsymplectic transformation M_{ns} must be integrated into the round to flat transformation section. This transformation anyway should be linear to preserve ϵ_{4d}. The section must also include an element M_t that decreases the horizontal emittance and increases the vertical one. This element might act as

$$\delta x' = -a \cdot x' \qquad \delta y' = b \cdot y', \qquad (a, b) > 0, \tag{11}$$

where a thin element not changing the particle position is assumed. The element imposes an effective linear friction in the horizontal plane and a linear heating in the vertical plane. If at the entrance to element M_t the distribution has large interplane coupling moments $\langle x'y \rangle$ and $\langle xy' \rangle$ imposed by preceding elements, the approximation

$$x' \approx \frac{\langle x'^2 \rangle}{\langle x'y \rangle} y \qquad y' \approx \frac{\langle y'^2 \rangle}{\langle xy' \rangle} x \tag{12}$$

turns Eq. (11) to

$$\delta x' \approx -a \frac{\langle x'^2 \rangle}{\langle x'y \rangle} y := q_s \cdot y \qquad \delta y' \approx b \frac{\langle y'^2 \rangle}{\langle xy' \rangle} x := q_s \cdot x \tag{13}$$

being the transformation of thin skew quadrupole with focusing strength

$$q_s = -a \frac{\langle x'^2 \rangle}{\langle x'y \rangle} \tag{14}$$

and

$$\frac{a}{b} = -\frac{\langle x'y \rangle}{\langle xy' \rangle} \cdot \frac{\langle y'^2 \rangle}{\langle x'^2 \rangle}, \tag{15}$$

implying that $\langle x'y \rangle$ and $\langle xy' \rangle$ need to differ in sign. The required condition of different signs of the moments $\langle x'y \rangle$ and $\langle xy' \rangle$ at the skew quadrupole entrance can be achieved by including a transformation

$$M_{\text{Sol Fringe}} = \begin{bmatrix} 1 & 0 & 0 & 0 \\ 0 & 1 & +K & 0 \\ 0 & 0 & 1 & 0 \\ -K & 0 & 0 & 1 \end{bmatrix} \tag{16}$$

through a solenoid fringe field into the beam line preceding the skew quadrupole with

$$K := \frac{B}{2(B\rho)}, \tag{17}$$

B as the solenoid on-axis magnetic field strength, and $(B\rho)$ as the beam rigidity. The K values at the entrance and exit fringe are equal in magnitude but they differ in sign. Solenoid fringe fields can provide the nonsymplectic transformation M_{ns} that preserves ϵ_{4d}. Summarizing, a round to flat transformation of an initial beam without interplane correlations can be achieved if it includes solenoidal fringe fields causing a nonsymplectic transformation M_{ns} and skew quadrupoles for the emittance transfer. This does not mean that the transformation can be achieved using just two elements: a fringe field and a single thin skew quadrupole. Both elements are essential ingredients but they are not sufficient. Apart from this it is physically not possible to create a stand alone fringe field since static magnetic field lines are closed, i.e., an entrance fringe field intrinsically causes an exit fringe field.

This section is concluded in mentioning briefly the concept of eigenemittances E as used in [8,10] and the references therein. The eigenemittances $\pm E_x$ and $\pm E_y$ of a four-dimensional transverse ion distribution solve the complex equation

$$\det(JC - iEI) = 0, \tag{3}$$

where I is the identity matrix. The eigenemittances are functions of the second beam moments and they do not change with symplectic transformations. But they do change by transformation through a solenoid fringe field. Their product is equal to ϵ_{4d} and for vanishing interplane coupling moments they are equal to the rms emittances. However, the eigenemittances of an ion beam should not be confused with those of an electron beam in rings being subject to damping and/or diffusion [11].

III. BEAMS EXTRACTED FROM AN ECR SOURCE

Round to flat transformation of ion beams extracted from an ECR source applies the same concept as this transformation of electron beams [1,2]. For ions it was proposed in [12] assuming a beam second moment matrix C with nonzero elements just along its two diagonals. But generally all coupling moments are different from zero and their magnitudes are similar. For electron and for ion beam extraction, the required nonsymplectic transformation M_{ns} is provided through placing the beam generation inside a longitudinal field region. For electrons a solenoid is installed around the cathode. In the case of ions the longitudinal field for plasma confinement is an intrinsic part of the ECR source. Prior to extraction the beam inside the plasma chamber is round ($\epsilon_x = \epsilon_y$) and is not correlated. After extraction along the solenoidal fringe field, the transverse phase space distribution from the source has interplane correlations. Figure 1 shows such a distribution for $^{16}O^{3+}$ extracted from the ECR source at GSI (Fig. 2) with an energy of 2.5 keV/u [13,14].

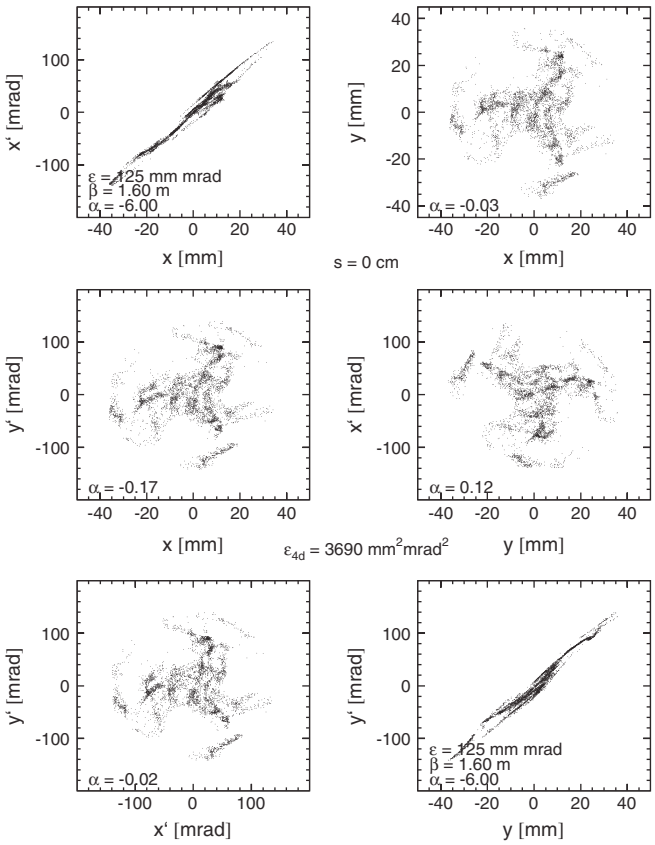

FIG. 1. Two-dimensional projections of the ECR transverse phase space distribution at the entrance to the emittance transfer section. Horizontal and vertical rms Twiss parameters are indicated as well as the four interplane correlation parameters.

The distribution is obtained from multiparticle simulations and beam measurements performed at the HLI are in good agreement with these simulations [14,15]. In Fig. 1 (and in the subsequent ones of same type) correlations between two coordinates u and v are indicated by the dimensionless α_{uv} parameter defined through the moments as

$$\alpha_{uv} := \frac{-\langle uv \rangle}{\sqrt{\langle u^2 \rangle \langle v^2 \rangle - \langle uv \rangle^2}}. \tag{18}$$

The 120° symmetry in the interplane projections is due to the nonlinear interplane coupling hexapolar field inside the ECR source. The observed interplane correlations α_{uv} are from the solenoidal fringe field and the signs of the beam moments $\langle x'y \rangle$ and $\langle xy' \rangle$ differ. Although the absolute values of the interplane α parameters seem small, the distribution is considerable correlated as seen by comparing the product of the two transverse emittances with the four-dimensional rms emittance [see Eqs. (6) and (8)], i.e. $\epsilon_x \cdot \epsilon_y = 4.2\epsilon_{4d}$. Because of the intrinsic interplane correlations the product $\epsilon_x \cdot \epsilon_y$ exceeds the value required from four-dimensional emittance preservation by a factor of about 4. That implies in turn that decreasing $\epsilon_x \cdot \epsilon_y$ by this factor can be achieved by just removing the interplane correlations from the beam using linear beam line elements.

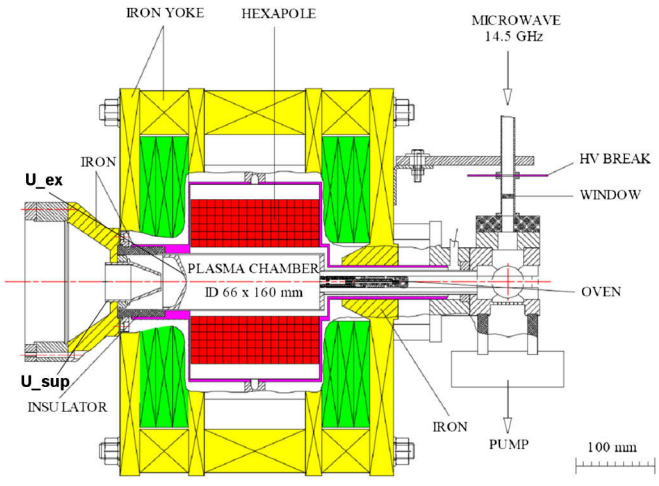

FIG. 2. ECR source at GSI with a permanent hexapole of 1 T at the pole tip. The longitudinal magnetic field is 1 T at maximum as well. It has an electron suppressing electrode at a potential of −2 kV. The extraction voltage is set to obtain 2.5 keV/u after extraction [24].

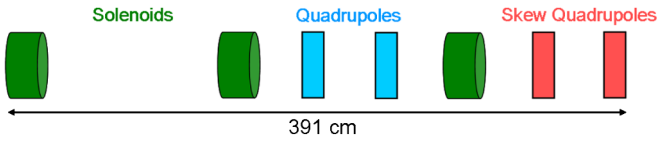

FIG. 3. Beam line from left to right for emittance transfer of a beam extracted from an ECR source (here the GSI HLI source). It comprises three solenoids, two quadrupoles, and two skew quadrupoles. Apertures are not to scale.

Figure 3 displays a beam line that removes the interplane correlations from the beam. It comprises three solenoids, two quadrupoles, and two skew quadrupoles. Its total length is about 4 m, the focusing strength is less than 0.5 m^{-1} (normal and skew quadrupoles) and 4.5 m^{-1} (solenoids). After extraction from the source the beam is divergent in both transverse planes. To provide simultaneous focusing in both planes, a solenoid is used as a first element of the beam line. The beam line needs to remove the four interplane correlation moments, minimize the vertical emittance (for instance) at its exit, and provide for beam envelopes within a reasonable aperture. In order to meet these boundaries simultaneously, several beam line elements are needed and we found that the beam line in Fig. 3 can do so. Finding the required focusing strengths is accomplished by numerical tools based on linear transport of the second beam moments [Eq. (7)]. As input the second moments extracted from the distribution shown in Fig. 1 has been used. Knowing the focusing strengths, multiparticle simulations using PARMTRA [16] have been done. Finite magnets with hard edges were used. The energy spread of the beam is very low but has been considered anyway. Space charge is of no concern at the HLI ECR source.

Simulated beam envelopes together with transverse rms emittances along the beam line are plotted in Fig. 4. The beam is round (equal emittances) until the entrance to the third solenoid. Behind the third solenoid the distribution has maximum correlation with $\epsilon_x \cdot \epsilon_y = 12.5\epsilon_{4d}$. Despite this high value the beam is not subject to losses. The emittances are dominated by wide angular spreads. Within the final skew quadrupole the correlations are almost completely removed. The distribution at the exit of the section is shown in Fig. 5. Its vertical rms emittance is about 13 times smaller than the horizontal one. Compared to its initial value the vertical rms emittance was decreased by 86% while the horizontal one increased by 85%. The absolute amount of emittance transfer, (−108 mm rad

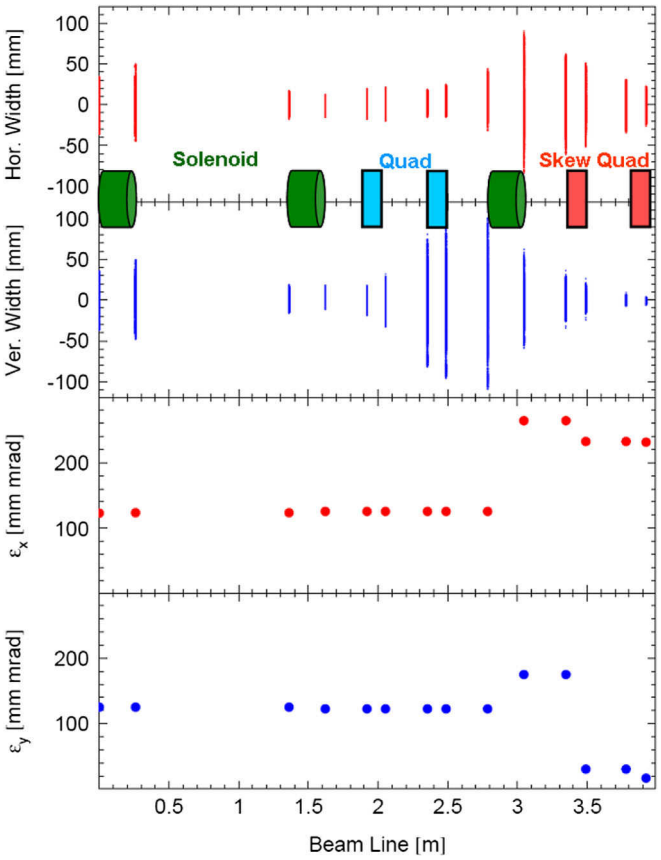

FIG. 4. From top to bottom: horizontal beam envelope, vertical beam envelope, horizontal rms emittance, and vertical rms emittance along the emittance transfer section for the ECR distribution.

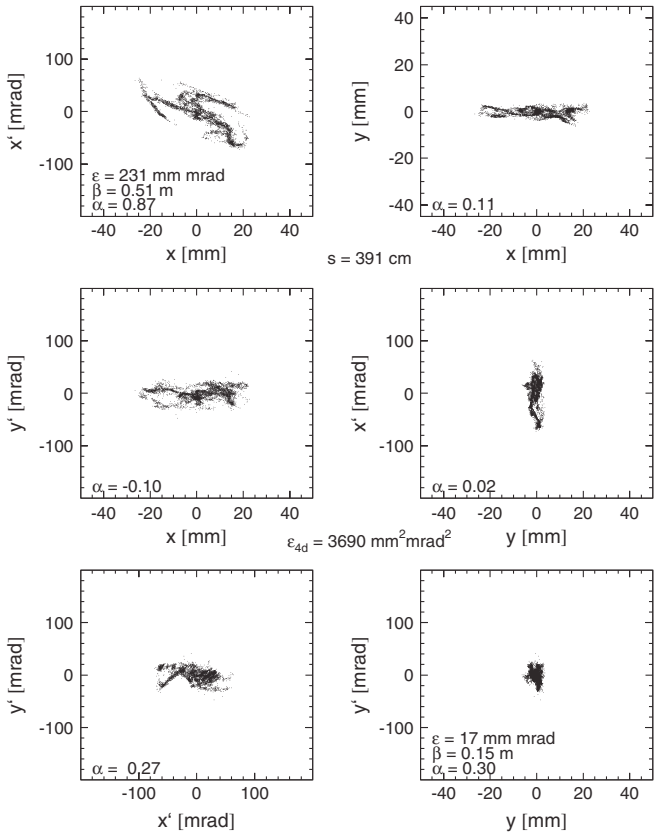

FIG. 5. Two-dimensional projections of the ECR transverse phase space distribution at the exit of the emittance transfer section. Horizontal and vertical rms Twiss parameters are indicated as well as the four interplane correlation parameters.

horizontally and +106 mm mrad vertically) is in excellent agreement to the value obtained analytically (±108 mm mrad) by applying Eq. (39) of [9] assuming an angular momentum dominated beam. The final rms emittances agree also well to the eigenemittances as evaluation of Eq. (3) delivers 230 mm mrad (E_x) and 16 mm mrad (E_y) at any position along the beam line. The product of the two transverse emittances was reduced from $4.2\epsilon_{4d}$ to $1.1\epsilon_{4d}$ while ϵ_{4d} was kept constant. The remaining factor of 1.1 as well as residual values of the interplane α parameters shows that the correlations were not completely removed. We attribute this to nonlinearities of the hexapolar coupling elements which cannot be fully removed by linear elements. Reducing correlations using hexapoles is proposed in [14].

IV. BEAMS TO BE STRIPPED

ECR sources generally do not provide high beam intensities for heavy and intermediate mass ions. Other source types are used in these cases (multicusp, metal vapor vacuum arc), which provide low charge states but high particle currents. From first principles also such sources can be designed applying ion extraction along a solenoidal fringe field to allow for later round to flat transformation. However, at extraction energy high intensity beam dynamics is subject to space charge forces. Latest at the entrance to an radio frequency quadrupole eventual space charge neutralization does not mitigate any longer the effect of beam self-fields. Acceleration and transport with space charge might strongly reduce or remove the required interplane correlation that was imposed previously at extraction along a solenoidal fringe field. For this reason the beam should be exposed to the fringe field after some acceleration, when space charge forces are sufficiently reduced. On the other hand, ion beams from low charge state, high particle current sources are stripped after gaining some energy in order to keep the acceleration process reasonable efficient.

The obstacle to meet is to provide for a nonsymplectic transformation M_{ns} after acceleration. Unlike in the ion source, the accelerated beam must enter and leave the solenoidal field and a complete solenoid is a symplectic transformation which cannot be used to prepare round to flat transformation.

The transformation through the solenoid is nonsymplectic if the beam rigidity is abruptly changed in between the entrance and exit fringe fields, i.e., if the beam properties are reset inside the solenoid. In this case the focusing strengths K from Eq. (16) are different at entrance and exit and the beam transport through the solenoid is a linear nonsymplectic transformation M_{ns} preserving ϵ_{4d}.

We propose to merge the required charge stripping of ions from low charge state, high particle current sources and the provision of a transformation M_{ns} for transverse emittance transfer preparation by placing the charge stripping foil in between two pancake coils as drawn in Fig. 6.

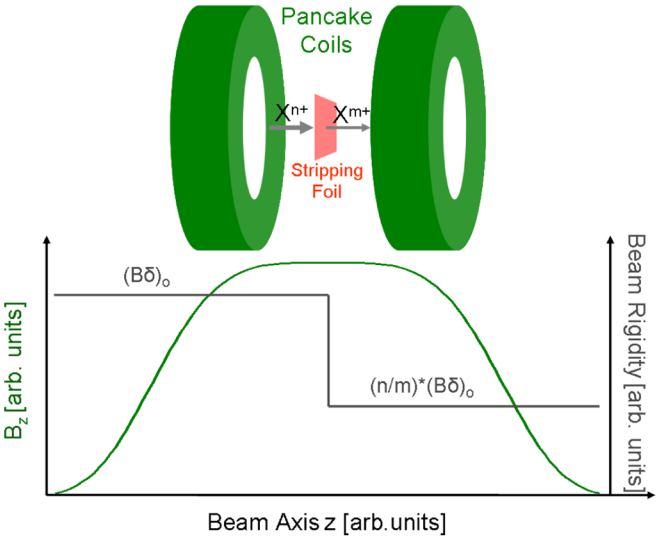

FIG. 6. Conceptual layout of an ion stripper setup providing a nonsymplectic transformation M_{ns} for later transverse emittance transfer. The stripping foil is placed between two pancake coils, i.e., inside a region with a longitudinal magnetic field of few Tesla in strength.

Stripping abruptly changes the beam rigidity and has to be performed anyway along the ion linac. Based on the existing charge stripping section of the GSI UNILAC, a beam line was conceptually designed that can provide horizontal to vertical emittance transfer.

The UNILAC (Fig. 7) comprises three source terminals, two drift tube linac (DTL) sections separated by a gaseous stripper section, and a transfer channel to the synchrotron SIS18. Along the DTL sections the beam is accelerated to 1.4 and 11.4 MeV/u, respectively. The transport channel to the synchrotron includes a foil stripper section shown in the photograph of Fig. 8. The foil stripper section [17] comprises a quadrupole singulet, a stripping foil, a vertical four bend chicane, and a quadrupole doublet. The chicane provides dispersion in its center for charge state separation. To demonstrate emittance transfer the beam line can be modified as drawn schematically in Fig. 9. GSI aims at experimental verification of the emittance transfer concept. The modifications of the existing foil stripper beam line will be conceived such that they do not intercept the beam in case no emittance transfer is required. The effective length of the longitudinal magnetic field region is 40 cm and the foil is placed 10 cm from the exit of this region.

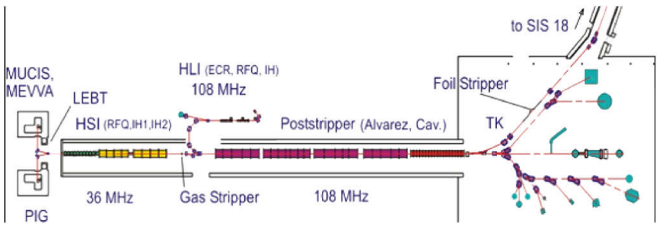

FIG. 7. The universal linear accelerator (UNILAC) at GSI.

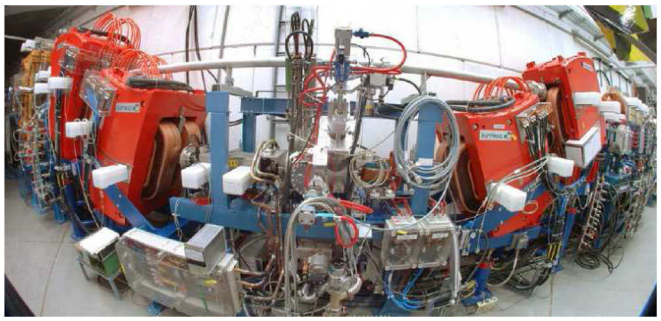

FIG. 8. Fish eye photograph of the foil charge state stripper at the GSI UNILAC including the four bend analyzing chicane. The beam enters from the left.

First beam tests are to be performed using a beam of H_3^+ stripped to a proton beam in a 20 μg/cm^2 carbon foil placed between to pancake coils. Protons were chosen in order to simplify the first proof of principles: low focusing strengths allow for usage of on-site equipment, low beam current avoids space charge effects, and a single charge state spectrum after stripping is provided. Multiparticle simulations for this case have been done and are presented in the following.

The change of charge state, i.e., rigidity, inside a longitudinal magnetic field region is modeled by matrix transformation of single particle coordinates according to Eq. (4). The matrix includes two parts M_{Sol_i} and M_{Sol_o}; the first part comprising a solenoid entrance fringe field and the longitudinal magnetic field until the stripping foil:

$$M_{\mathrm{Sol}_i} = \begin{bmatrix} 1+\frac{KL(1-C)}{\alpha} & \frac{SL}{\alpha} & \frac{SLK}{\alpha} & -\frac{L(1-C)}{\alpha} \\ KS & C & CK & -S \\ -\frac{SLK}{\alpha} & \frac{L(1-C)}{\alpha} & 1+\frac{KL(1-C)}{\alpha} & \frac{SL}{\alpha} \\ -CK & S & SK & C \end{bmatrix} \tag{19}$$

with

$$C := \cos(KL), \qquad S := \sin(KL), \qquad \alpha := 2KL, \tag{20}$$

K from Eq. (16), and L as distance from the effective longitudinal field edge to the foil. The beam rigidity is calculated from the unstripped charge state, i.e., using H_3^+ at 11.4 MeV/u. The foil itself is modeled by increasing the spread of the angular distribution through scattering, i.e.,

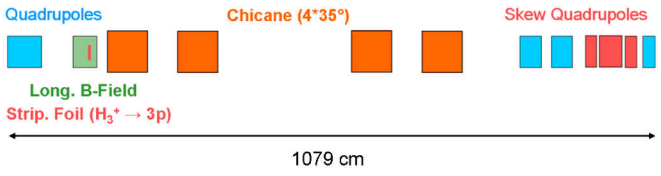

FIG. 9. Beam line from left to right for emittance transfer of a beam along the UNILAC. It comprises two quadrupole singulets, a stripping foil in between two pancake coils, a four bend chicane, a doublet, and a skew quadrupole triplet. Apertures are not to scale.

$$\langle x'^2\rangle + \langle y'^2\rangle \rightarrow \langle x'^2\rangle + \langle y'^2\rangle + \Delta\varphi^2. \tag{21}$$

The amount of scattering $\Delta\varphi$ was calculated using the ATIMA code [18] as 0.296 mrad. Because of scattering the four-dimensional emittance ϵ_{4d} increases during the stripping process. Transport from the foil to the exit of the longitudinal magnetic field region is modeled by a matrix corresponding to M_{Sol_i}, i.e.,

$$M_{\mathrm{Sol}_o} = \begin{bmatrix} 1 & \frac{SL}{\alpha} & 0 & -\frac{L(1-C)}{\alpha} \\ 0 & C-\frac{KL(1-C)}{\alpha} & -K & -S-\frac{SLK}{\alpha} \\ 0 & \frac{L(1-C)}{\alpha} & 1 & \frac{SL}{\alpha} \\ K & \frac{SLK}{\alpha}+S & 0 & C-\frac{KL(1-C)}{\alpha} \end{bmatrix} \tag{22}$$

using the beam rigidity corresponding to the stripped beam, i.e., protons at 11.4 MeV/u. Here L is the distance from the foil to the exit of the longitudinal magnetic field region. According to [18], the energy loss and straggling in the foil can be neglected. It must be emphasized that the increase of ϵ_{4d} is purely from scattering in the foil; it is not caused by the change of beam rigidity inside the longitudinal field. Scattering in the foil occurs anyway along beam

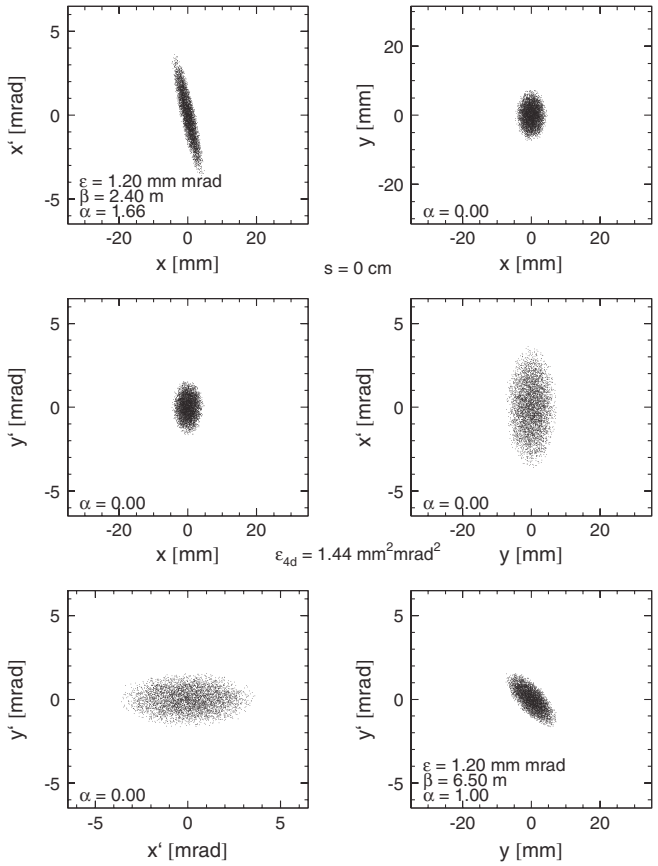

FIG. 10. Two-dimensional projections of the transverse phase space distribution at the entrance to the proposed emittance transfer section along the UNILAC. Horizontal and vertical rms Twiss parameters are indicated as well as the four interplane correlation parameters.

lines that include foil strippers. The simulations additionally included beam momentum spread, hexapolar fringe fields of the chicane dipoles, and the existing aperture limitations.

Simulations started at the entrance to the quadrupole singulet in front of the chicane. Figure 10 shows the initial transverse phase space distribution. Initial six-dimensional Twiss parameters were concluded from various beam experiments with H_3^+ beams. Beam spot images from fluorescence screens close to this position did not reveal any x-y correlation. Therefore initial interplane correlations are assumed as zero. The distribution was tracked through the emittance transfer section and corresponding envelopes and transverse emittances are plotted in Fig. 11. Full beam transmission is achieved. The observed increase in both transverse emittances at the entrance to the longitudinal magnetic field region is driven by interplane correlations caused by the fringe field. There is no increase of the four-dimensional emittance ϵ_{4d} until the stripping foil. However, the increase of ϵ_{4d} at the foil from scattering is just 4%. Vertical dispersion from the first dipole causes additional increase of the vertical and the four-dimensional emittance, both being compensated later by the last dipole.

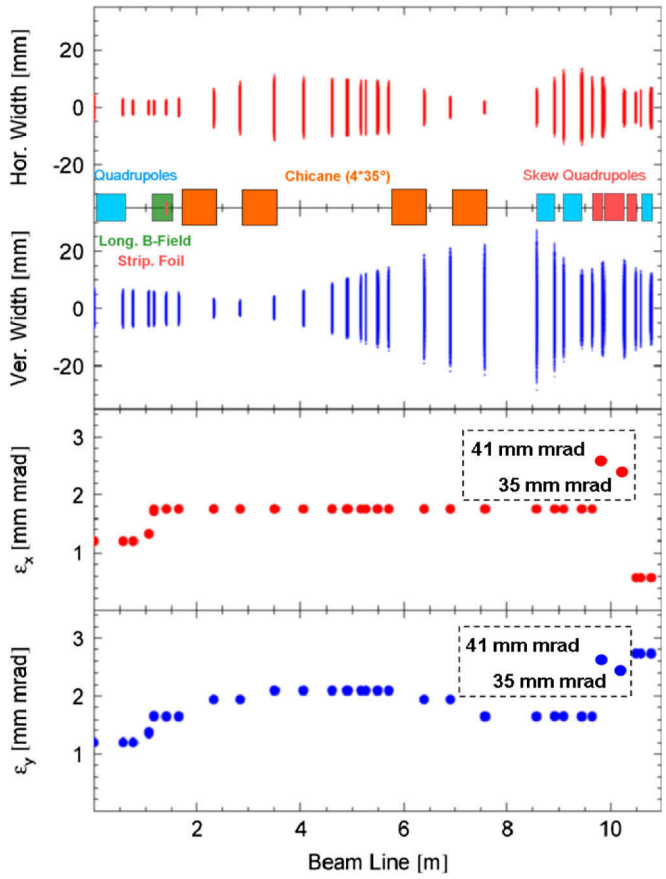

FIG. 11. From top to bottom: horizontal beam envelope, vertical beam envelope, horizontal rms emittance, and vertical rms emittance along the proposed emittance transfer section along the UNILAC.

The distribution at the exit of the longitudinal magnetic field region is shown in Fig. 12. It has interplane correlations and the signs of $\langle x'y\rangle$ and $\langle xy'\rangle$ differ as expected from the action of the solenoidal fringe fields. The product of the transverse emittances is a factor of 1.8 larger than the four-dimensional emittance ϵ_{4d}. During the transport through the chicane the horizontal emittance is preserved. The intrinsic interplane correlation of the beam, i.e., the ratio $\epsilon_x\epsilon_y/\epsilon_{4d}$ (corrected wrt vertical dispersion) remains constant. Along the elements after the chicane the correlations are removed, the horizontal emittance is minimized, and the beam is rematched for further transport to the synchrotron. To accomplish these tasks within the existing apertures, the gradients of the quadrupole doublet, the skew triplet, and the final singulet are determined numerically. The same algorithm as mentioned in Sec. III is applied. As input for the algorithm the second beam moments extracted from the distribution at the doublet entrance are used (Fig. 13). Here we presently rely on the simulations using the PARMTRA code being part of the PARMILA code family [19]. The later has been benchmarked successfully with beam experiments involving

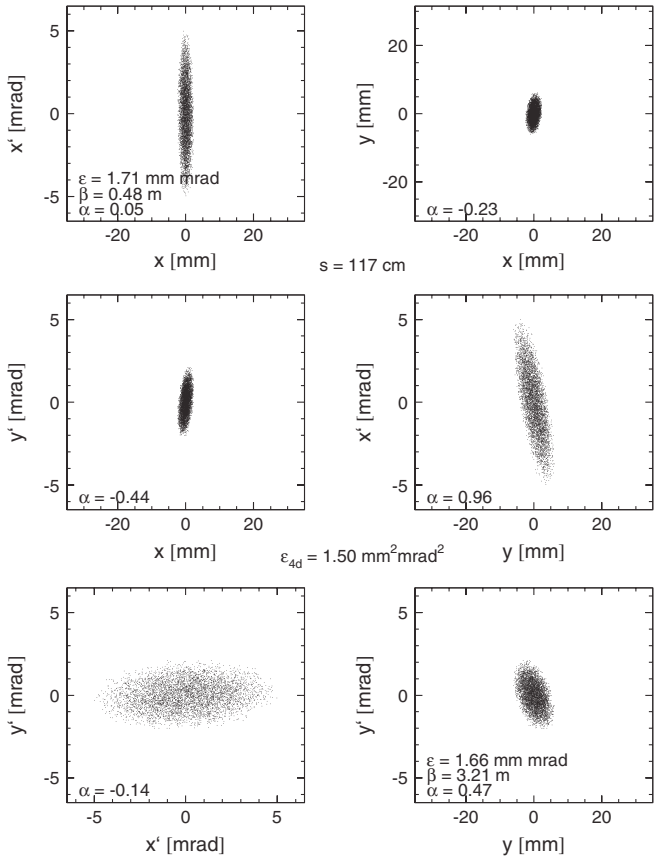

FIG. 12. Two-dimensional projections of the transverse phase space distribution at the exit of the longitudinal magnetic field section of the proposed emittance transfer section along the UNILAC. Horizontal and vertical rms Twiss parameters are indicated as well as the four interplane correlation parameters.

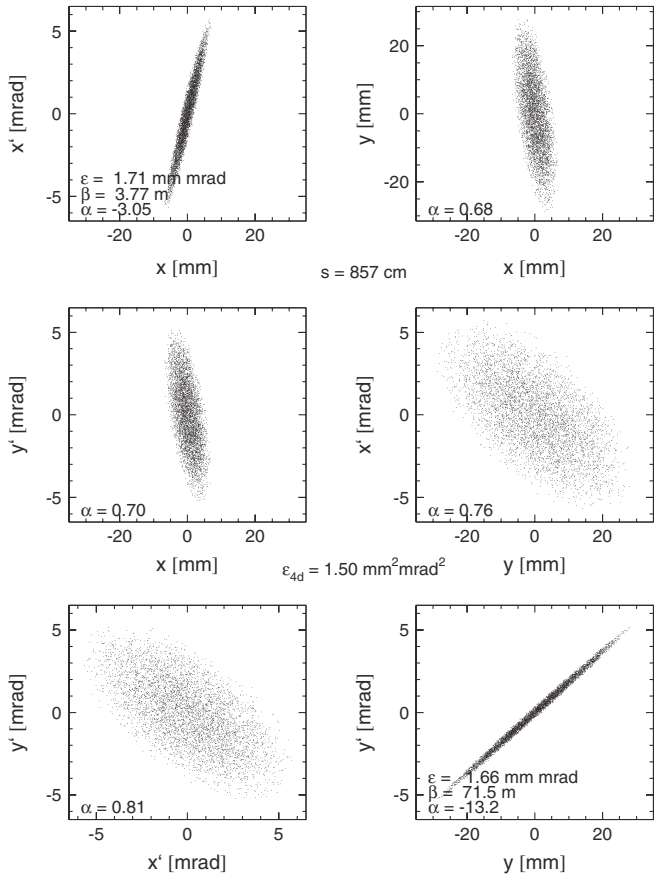

FIG. 13. Two-dimensional projections of the transverse phase space distribution at the entrance to the first quadrupole after the chicane of the proposed emittance transfer section along the UNILAC. Horizontal and vertical rms Twiss parameters are indicated as well as the four interplane correlation parameters.

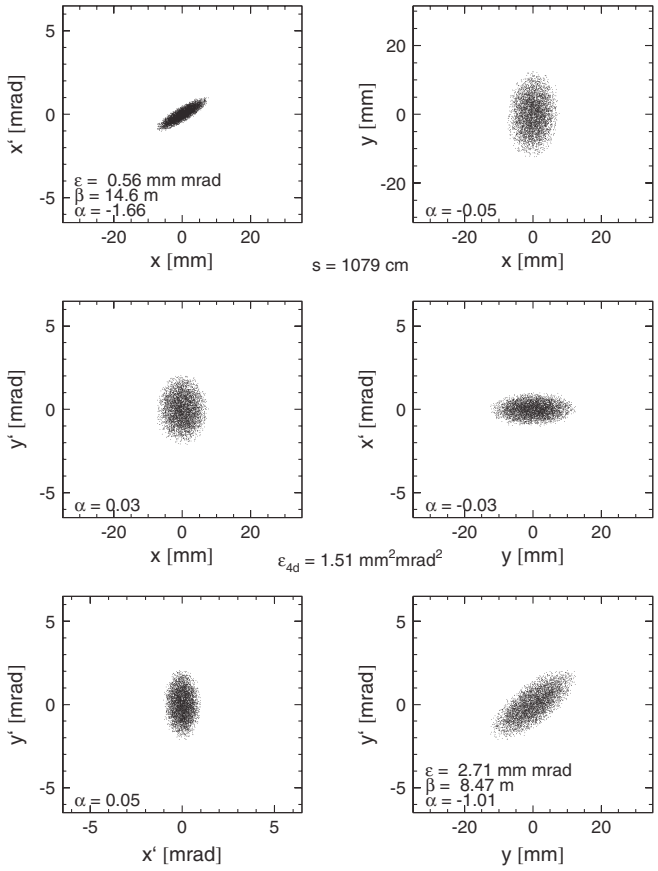

FIG. 14. Two-dimensional projections of the transverse phase space distribution at the exit of the proposed emittance transfer section along the UNILAC. Horizontal and vertical rms Twiss parameters are indicated as well as the four interplane correlation parameters.

more complex beam lines even with strong space charge [20,21]. The beam moments at the doublet entrance also can be measured if a pepper-pot device will be installed right behind the last singulet. Its installation is planned for the experimental verification of the proposed emittance transfer concept.

After applying the required gradients for emittance transfer and horizontal emittance minimization, the beam is transported until the exit of the last singulet. The resulting distribution is plotted in Fig. 14. Interplane correlations are almost completely removed. Residual values are due to hexapolar dipole fringe fields as well as to chromaticity in quadrupoles and skew quadrupoles from the finite beam momentum spread ($\approx 0.1\%$ rms). The product of $\epsilon_x \cdot \epsilon_y$ exceeds ϵ_{4d} by less than 1%. Starting from an initial transverse emittance ratio of 1.0, the final ratio is 4.8. The horizontal emittance is reduced by 53% and the vertical one increased by 125%. The four-dimensional emittance ϵ_{4d} increased by 5% mainly due to angular scattering in the stripper foil (4%). The remaining part is from beam line nonlinearities as mentioned before. The achieved amount of emittance transfer is -0.64 mm mrad horizontally and $+1.51$ mm mrad vertically. The corresponding analytical value for an angular momentum dominated beam [Eq. (39) of [9]] is 1.65 mm mrad. This shows that the beam correlation moments at the exit of the longitudinal magnetic field region are not dominated by angular momentum although they include angular momentum.

Unlike for the round to flat transformation of beams from an ECR source (Sec. III), the longitudinal field strength at the stripper foil is a free parameter. The amount of emittance transfer scales with the field strength. However, practical limitations for this amount rise from finite apertures. Finally, the eigenemittances of the beam distributions were evaluated along the beam line. The result is listed in Table I. The eigenemittances change just along the nonsymplectic transformations, i.e. the entrance and exit longitudinal fringe field and the stripping foil.

TABLE I. Eigenemittances along the proposed rms emittance transfer section along the UNILAC.

Position	E_x/E_y [mm mrad]
Entrance	1.2/1.2
In front of foil, behind entrance fringe	1.8/0.8
Behind foil, in front of exit fringe	1.9/0.8
Behind exit fringe	2.7/0.6

V. CONCLUSION AND OUTLOOK

It was shown that flat to round transformation is not restricted to electron beams but can be accomplished for beams of ions as well. The required solenoid fringe fields are provided intrinsically for beams being extracted from an ECR source. Beams from other sources can be emittance shaped by applying charge state stripping inside a longitudinal magnetic field. Examples for the layout of emittance transfer beam lines were presented for both cases. Multiparticle simulations demonstrated that the transfer is feasible. An initial round beam could be transformed into a beam with transverse emittance ratio of almost five. The amount of transfer for stripped ions can be controlled through the longitudinal magnetic field strength.

GSI aims at experimental verification of emittance transfer by assembling the beam lines presented in this paper. Emittance transfer of beams from ECR sources might by of special interest for facilities operating an ECR source in connection with multiturn injection into a synchrotron, as cancer treatment facilities for instance [22]. High intensity beams of intermediate or heavy mass ions for synchrotrons are to be provided for the FAIR project [23]. Stripping of those ions results in a charge state spectrum and requires charge state separation. Additionally, stripping of heavy ions uses much thicker foils ($\approx 600\ \mu g/cm^2$) with respect to light ions, thus the four-dimensional emittance growth from scattering is significantly higher ($\geq 70\%$). This growth reduces the budget for the amount of emittance transfer. However, emittance transfer lines can be designed also for such scenarios although the layout will be more complex than the one for protons presented here. Tentative layouts were made on the emittance transfer for beams of $^{238}U^{27+}$ stripped to $^{238}U^{73+}$ based on the existing foil stripping section at the GSI UNILAC. Horizontal emittance reduction of up to 40% was achieved including space charge and charge state separation. Further optimization of the layout for an emittance transfer section for intense beams of heavy ions is needed. This optimization is beyond the scope of the present paper.

ACKNOWLEDGMENTS

The author wishes to express his gratitude to L. Dahl, S. Ratschow, and the ECR source team at GSI for fruitful discussions.

[1] R. Brinkmann, Y. Derbenev, and K. Flöttmann, Phys. Rev. ST Accel. Beams **4**, 053501 (2001).
[2] D. Edwards, H. Edwards, N. Holtkamp, S. Nagaitsev, J. Santucci, R. Brinkmann, K. Desler, K. Flöttmann, I. Bohnet, and M. Ferrario, in *Proceedings of the XX Linear Accelerator Conference, Monterey, CA*, edited by A. Chao, eConf C000821 (2000).
[3] P. J. Bryant, CAS–CERN Accelerator School (CERN, Geneva, Switzerland, 1986), Vol. 15, p. 157.
[4] A. Burov, S. Nagaitsev, and Y. Derbenev, Phys. Rev. E **66**, 016503 (2002).
[5] K. L. Brown and R. V. Servranckx, Stanford Linear Accelerator Center Technical Report No. slac-pub-4679, 1989.
[6] D. Edwards and L. Teng, IEEE Trans. Nucl. Sci. **20**, 885 (1973).
[7] F. Willeke and G. Ripken, AIP Conf. Proc. **184**, 758 (1989).
[8] V. A. Lebedev and S. A. Bogacz, JINST **5**, P10010 (2010).
[9] K.-J. Kim, Phys. Rev. ST Accel. Beams **6**, 104002 (2003).
[10] Bruce E. Carlsten, Kip A. Bishofberger, Leanne D. Duffy, Steven J. Russell, Robert D. Ryne, Nikolai A. Yampolsky, and Alex J. Dragt, Phys. Rev. ST Accel. Beams **14**, 050706 (2011).
[11] A. Franchi, L. Farvacque, J. Chavanne, F. Ewald, B. Nash, K. Scheidt, and R. Tomás, Phys. Rev. ST Accel. Beams **14**, 034002 (2011).
[12] P. Bertrand, J. P. Biarrotte, and D. Uriot, in *Proceedings of the 10th European Accelerator Conference, Edinburgh, Scotland*, edited by J. Poole and C. Petit-Jean-Genaz (Institute of Physics, Edinburgh, Scotland, 2006).
[13] P. Spädtke (private communication).
[14] P. Spädtke, R. Lang, J. Mäder, F. Maimone, J. Rossbach, K. Tinschert, and J. Stetson, in *Proceedings of the IPAC'10 Conference, Kyoto, Japan*, edited by A. Noda (ICR, Kyoto, 2010).
[15] P. Spädtke, R. Lang, J. Mäder, J. Rossbach, and K. Tinschert, in *Proceedings of the XXIV Linear Accelerator Conference, Victoria, BC, Canada*, edited by M. Comyn (TRIUMF, Victoria, 2008).
[16] J. Struckmeier, GSI Helmholtzzentrum für Schwerionenforschung GmbH Technical Report No. gsi-esr-87-03, 1998.
[17] W. Barth, L. Dahl, L. Groening, P. Gerhard, S. Mickat, and M. S. Kaiser, in Proceedings of the XXIV Linear Accelerator Conference, Victoria, BC, Canada (Ref. [15]).
[18] H. Weick, "Atima, calculate atomic interaction with matter," http://www-linux.gsi.de/~weick/atima/atima.html.
[19] J. Billen and H. Takeda, Technical Report No. LAUR-98-4478, Los Alamos, 1998) (revised 2004).
[20] L. Groening, W. Barth, W. Bayer, G. Clemente, L. Dahl, P. Forck, P. Gerhard, I. Hofmann, G. Riehl, S. Yaramyshev, D. Jeon, and D. Uriot, Phys. Rev. ST Accel. Beams **11**, 094201 (2008).
[21] L. Groening, W. Barth, W. Bayer, G. Clemente, L. Dahl, P. Forck, P. Gerhard, I. Hofmann, M. S. Kaiser, M. Maier, S. Mickat, T. Milosic, D. Jeon, and D. Uriot, Phys. Rev. Lett. **102**, 234801 (2009).
[22] T. Haberer, J. Debus, H. Eickhoff, O. Jäkel, D. Schulz-Ertner, and U. Weber, Radiother. Oncol **73**, S186 (2004).
[23] FAIR Baseline Technical Report (Vol. 2), GSI Helmholtzzentrum für Schwerionenforschung GmbH, 2006.
[24] K. Tinschert (private communication).